

Shape-phase transitions in nuclei and random interactions *

Roelof Bijker

ICN-UNAM, AP 70-543, 04510 México D.F., México

E-mail: bijker@nuclecu.unam.mx

Abstract

In these lecture notes I present a short review of nuclear shapes, shape coexistence and shape-phase transitions in the interacting boson model. In a study with random interactions it is shown that the appearance of regular spectral features is a far more common phenomenon than was previously thought. The origin of these features are explained by studying the relation with the underlying geometric shapes.

1 Introduction

The concept of shape coexistence and shape-phase transitions in atomic nuclei is currently a topic of active research both experimentally and theoretically [1, 2]. The phenomenon of shape coexistence refers to the occurrence of different shapes in a given nucleus and has been observed in fission isomers in the actinides, intruder orbitals in or near closed (sub)shell nuclei and superdeformed nuclei at high spins [3]. Whereas coexisting shapes are usually associated with different configurations (*e.g.* normal and intruder), shape-phase transitions describe how one geometric shape evolves into another within the same configuration, *e.g.* between spherical and deformed shapes in the Nd, Sm and Gd nuclei or between γ -soft and deformed in the Pt-Os mass region [4].

It is the aim of these lecture notes to present a short overview of shape-phase transitions in the interacting boson model (IBM) and its extensions and to discuss the appearance of regular spectral features from the IBM with random interactions and its relation with the underlying geometric shapes and critical points. In the first lecture (Section 2), I present a review of shape-phase transitions for the IBM including two more recent developments, *i.e.* two-neutron transfer reactions as a probe of shape-phase coexistence in the Ge isotopes and the shape-phase diagram for the neutron-proton IBM. In the second lecture, I discuss some surprising results that were obtained in studies of the IBM with random interactions: the predominance of ground states with angular momentum $L = 0$ and the occurrence of both vibrational and rotational structures despite the random nature of the interactions.

*Lecture notes: IV International Balkan School on Nuclear Physics, Bodrum, Turkey, September 22-29, 2004

2 Shape-phase transitions in nuclei

Shape-phase transitions in atomic nuclei were studied extensively in the early 80's in the framework of the IBM. The general procedure was laid out by Gilmore in the 70's using atomic coherent states [5] in combination with catastrophe theory [6] which was applied to nuclear physics by Dieperink, Scholten and Iachello [4], Feng, Gilmore and Deans [7] and López-Moreno and Castaños [8]. After the introduction of critical point symmetries as special solutions to the Bohr Hamiltonian [9, 10], the subject of shape-phase transitions has witnessed a revival both experimentally and theoretically. For a recent review of shape-phase transitions and critical point symmetries in nuclear physics, see [2].

2.1 The interacting boson model

The IBM provides an elegant and powerful tool for the description of collective nuclei [11]. In this model, collective excitations in nuclei are described in terms of a system of N interacting monopole (s^\dagger) and quadrupole (d_m^\dagger with $m = 0, \pm 1, \pm 2$) bosons with $L^P = 0^+$ and 2^+ , respectively. The the number of bosons N is determined by half the number of valence nucleons. In addition to N , the eigenfunctions have good angular momentum and parity L^P . Let's consider the schematic IBM Hamiltonian of the consistent-Q formulation (CQF) [12]

$$H = \epsilon \hat{n}_d - \kappa \hat{Q}(\chi) \cdot \hat{Q}(\chi) , \quad (1)$$

where \hat{n}_d is the number operator for quadrupole bosons

$$\hat{n}_d = \sqrt{5} (d^\dagger \times \tilde{d})^{(0)} , \quad (2)$$

and $\hat{Q}(\chi)$ denotes the quadrupole operator

$$\hat{Q}_m(\chi) = (s^\dagger \times \tilde{d} + d^\dagger \times \tilde{s})_m^{(2)} + \chi (d^\dagger \times \tilde{d})_m^{(2)} . \quad (3)$$

Here $\tilde{s} = s$ and $\tilde{d}_m = (-1)^{2-m} d_{-m}$. The Hamiltonian of Eq. (1) describes the main features of collective nuclei: it contains the dynamical symmetries of the IBM for special choices of the coefficients ϵ , κ and χ , and allows to describe the transitional regions between any of symmetry limits as well.

2.2 Potential-energy surface

The connection between the IBM, potential-energy surfaces, geometric shapes and phase transitions can be investigated by introducing a coherent, or intrinsic, state which is expressed as a boson condensate [4]

$$|N, \beta, \gamma\rangle = \frac{1}{\sqrt{N!}} (b_c^\dagger)^N |0\rangle , \quad (4)$$

with

$$b_c^\dagger = \frac{1}{\sqrt{1+\beta^2}} \left(s^\dagger + \beta \cos \gamma d_0^\dagger + \frac{1}{\sqrt{2}} \beta \sin \gamma (d_2^\dagger + d_{-2}^\dagger) \right) , \quad (5)$$

where the variables β and γ determine the geometry of the nuclear surface. Spherical shapes are characterized by $\beta = 0$ and deformed ones by $\beta > 0$. The angle γ allows one to distinguish between axially deformed nuclei, $\gamma = 0^\circ$ for prolate and $\gamma = 60^\circ$ for oblate deformation, and triaxial nuclei $0^\circ < \gamma < 60^\circ$.

The potential-energy surface is given by the expectation value of the Hamiltonian in the coherent state [4]

$$\begin{aligned} V(\beta, \gamma) &= \langle N, \beta, \gamma | : H : | N, \beta, \gamma \rangle \\ &= \frac{\epsilon N \beta^2}{1 + \beta^2} - \frac{\kappa N(N-1)}{(1 + \beta^2)^2} \left[4\beta^2 - 4\chi \sqrt{\frac{2}{7}} \beta^3 \cos 3\gamma + \frac{2}{7} \chi^2 \beta^4 \right]. \end{aligned} \quad (6)$$

The normal ordered form of the Hamiltonian $: H :$ was used to eliminate the contributions of the one-body terms of the quadrupole-quadrupole interaction to the energy surface $V(\beta, \gamma)$.

The equilibrium shape associated to the IBM Hamiltonian can be obtained by determining the minimum of the energy surface with respect to the geometric variables β and γ , *i.e.* the first derivatives vanish

$$\frac{\partial V}{\partial \beta} = \frac{\partial V}{\partial \gamma} = 0, \quad (7)$$

and the determinant of the Hessian matrix of the second derivatives is positive

$$\left(\frac{\partial^2 V}{\partial \beta^2} \right) \left(\frac{\partial^2 V}{\partial \gamma^2} \right) - \left(\frac{\partial^2 V}{\partial \beta \partial \gamma} \right)^2 > 0. \quad (8)$$

2.3 Dynamical symmetries

First some general properties of the IBM are reviewed, in particular the equilibrium shapes for the dynamical symmetries that arise for special choices of the coefficients ϵ , κ and χ in the Hamiltonian of Eq. (1). A more detailed discussion can be found in [11].

The $U(5)$ limit

For $\kappa = 0$, the Hamiltonian H of Eq. (1) reduces to the $U(5)$ limit of the IBM

$$H_1 = \epsilon \hat{n}_d. \quad (9)$$

The potential-energy surface of H_1 is given by

$$V_1(\beta) = \frac{\epsilon N \beta^2}{1 + \beta^2}. \quad (10)$$

The equilibrium value of the deformation parameter β is easily obtained by solving Eqs. (7) and (8) to give $\beta_e = 0$ which corresponds to a spherical shape.

The $SO(6)$ limit

For $\epsilon = 0$ and $\chi = 0$, one recovers the the $SO(6)$ limit

$$H_2 = -\kappa \hat{Q}(\chi) \cdot \hat{Q}(\chi), \quad \chi = 0. \quad (11)$$

Also in this case, the energy surface only depends on β

$$V_2(\beta) = -\frac{4\kappa N(N-1)\beta^2}{(1+\beta^2)^2}. \quad (12)$$

The equilibrium value is given by $\beta_e = 1$ corresponding to a γ -unstable deformed shape.

The $SU(3)$ limit

For $\epsilon = 0$ and $\chi = \mp\sqrt{7}/2$, the schematic Hamiltonian of Eq. (1) reproduces the $SU(3)$ limit

$$H_3 = -\kappa \hat{Q}(\chi) \cdot \hat{Q}(\chi), \quad \chi = \mp\frac{1}{2}\sqrt{7}. \quad (13)$$

For this case, the potential-energy surface depends both on β and γ

$$V_3(\beta, \gamma) = -\frac{\kappa N(N-1)}{(1+\beta^2)^2} \left[4\beta^2 \pm 2\sqrt{2}\beta^3 \cos 3\gamma + \frac{1}{2}\beta^4 \right]. \quad (14)$$

The equilibrium values are given by $\beta_e = \sqrt{2}$ and $\gamma_e = 0^\circ$ for $\chi = -\frac{1}{2}\sqrt{7}$ and by $\beta_e = \sqrt{2}$ and $\gamma_e = 60^\circ$ for $\chi = \frac{1}{2}\sqrt{7}$ corresponding to prolate and oblate deformed shapes, respectively.

2.4 Shape-phase transitions

The transitional regions between any two of the dynamical symmetries of the IBM can be studied by combining the corresponding Hamiltonians, and varying the relative strength of the interaction terms. In 1980, Dieperink, Scholten and Iachello showed that these transitional regions exhibit shape-phase transitions [4].

In 1996, the subject was revisited by López-Moreno and Castaños [8] who investigated the shape-phase transitions for general (one- and two-body) IBM Hamiltonians using the full power of catastrophe theory [13]. It was shown that the shape-phase diagram depends on two independent combinations of the parameters of the IBM Hamiltonian, called r_1 and r_2 , which can be used to classify the equilibrium configurations. For the Hamiltonian of Eq. (1) they are given by

$$r_1 = \frac{-4 + \frac{\epsilon}{\kappa(N-1)}}{-\frac{4}{7}\chi^2 + 4 + \frac{\epsilon}{\kappa(N-1)}}, \quad r_2 = \frac{-8\chi\sqrt{\frac{2}{7}}}{-\frac{4}{7}\chi^2 + 4 + \frac{\epsilon}{\kappa(N-1)}}. \quad (15)$$

In addition, closed analytic expressions were derived for the separatrix, which consists of the critical points

$$r_{1c} = -\frac{1}{2} + \frac{1}{2}\sqrt{1 + \frac{1}{2}r_2^2}, \quad (16)$$

Table 1: Equilibrium values of the deformation parameters for the dynamical symmetry limits of the IBM.

| Limit | ϵ | κ | χ | r_1 | r_2 | β_e | γ_e |
|---------|------------|----------|------------------------|----------------|------------------------|------------|------------|
| $U(5)$ | ϵ | 0 | - | 1 | 0 | 0 | - |
| $SO(6)$ | 0 | κ | 0 | -1 | 0 | ± 1 | - |
| $SU(3)$ | 0 | κ | $-\frac{1}{2}\sqrt{7}$ | $-\frac{4}{3}$ | $\frac{4}{3}\sqrt{2}$ | $\sqrt{2}$ | 0° |
| | 0 | κ | $+\frac{1}{2}\sqrt{7}$ | $-\frac{4}{3}$ | $-\frac{4}{3}\sqrt{2}$ | $\sqrt{2}$ | 60° |

the spinodal and antispinodal points

$$r_{1s} = -1 + \frac{(9r_2^2 + 16)^{3/2} - 64}{54r_2^2}, \quad r_{1a} = 0. \quad (17)$$

In Table 1 the values of r_1 and r_2 are given for each of the dynamical symmetries discussed in the previous section.

The methods used in [4] and [8] are closely related and give complementary results, which lead to a very simple and clear picture of the shape-phase diagram in nuclei as will be shown in the remainder of this section.

The $U(5) - SO(6)$ transitional region

The transition between the spherical and γ -unstable deformed shapes can be studied by considering the Hamiltonian

$$H_{12} = H_1 + H_2 = \epsilon \hat{n}_d - \kappa \hat{Q}(0) \cdot \hat{Q}(0). \quad (18)$$

The corresponding energy surface can be written as

$$\mathcal{E}(\beta) = \frac{V_1(\beta) + V_2(\beta)}{N\epsilon} = \frac{\beta^2}{1 + \beta^2} - 4\eta \frac{\beta^2}{(1 + \beta^2)^2}, \quad (19)$$

where the energy functionals of Eqs. (10) and (12) were scaled by ϵ and the number of bosons N . The transition is described by varying the control parameter $\eta = \kappa(N - 1)/\epsilon$ on the interval $0 \leq \eta < \infty$. The equilibrium value of β depends on η

$$\begin{aligned} \eta \leq \frac{1}{4} & : & \beta_e &= 0, \\ \eta \geq \frac{1}{4} & : & \beta_e^2 &= \frac{4\eta - 1}{4\eta + 1}, \end{aligned} \quad (20)$$

i.e. a spherical minimum for $\eta \leq 1/4$ and a deformed one for $\eta > 1/4$. The phase transition takes place at the critical point $\eta_c = 1/4$. Its nature can be determined by studying the ground state energy $\mathcal{E}_{\min}(\eta) = \mathcal{E}(\beta_c)$ and its derivatives at the critical point [6]: if the ground state energy is discontinuous in the control parameter η the transition is zeroth order, and if the first (second) derivative is discontinuous it is first (second) order. The ground state energy of Eq. (19) is

$$\begin{aligned} \eta \leq \frac{1}{4} & : & \mathcal{E}_{\min}(\eta) &= 0 , \\ \eta \geq \frac{1}{4} & : & \mathcal{E}_{\min}(\eta) &= -\frac{(4\eta - 1)^2}{16\eta} . \end{aligned} \quad (21)$$

The first derivative is continuous at $\eta_c = 1/4$, whereas the second derivative is discontinuous. Therefore, the $U(5)$ - $SO(6)$ transitional region exhibits a second-order phase transition [4].

An analysis in terms of catastrophe theory gives that the values of r_1 and r_2 for the Hamiltonian of Eq. (18) are given by

$$r_1 = \frac{1 - 4\eta}{1 + 4\eta}, \quad r_2 = 0 . \quad (22)$$

In the r_2 - r_1 plane the transitional region for $0 \leq \eta < \infty$ is represented by $-1 \leq r_1 \leq 1$ and $r_2 = 0$. The critical, antispinodal and spinodal points are obtained by taking the intersection with the curves corresponding to Eqs. (16) and (17)

$$\begin{aligned} \eta_c &= \frac{1}{4}, & r_{1c} &= r_{2c} = 0 , \\ \eta_a &= \frac{1}{4}, & r_{1a} &= r_{2a} = 0 , \\ \eta_s &= \frac{1}{4}, & r_{1s} &= r_{2s} = 0 . \end{aligned} \quad (23)$$

This shows that the critical, antispinodal and spinodal points coincide which is a signature for a second-order phase transition, in agreement with the results obtained above from the analysis of the ground state energy [4]. In the left panel of Fig. 1, the potential-energy surface is given for three different values of the control parameter η . For $\eta < \eta_c$ the equilibrium shape is spherical and for $\eta > \eta_c$ it is deformed. There is no region of coexistence of spherical and deformed minima.

The $U(5) - SU(3)$ transitional region

The transitional region between the spherical and axially deformed nuclei can be studied by considering the schematic Hamiltonian

$$H_{13} = H_1 + H_3 = \epsilon \hat{n}_d - \kappa \hat{Q}(\chi) \cdot \hat{Q}(\chi), \quad \chi = \mp \frac{1}{2} \sqrt{7}, \quad (24)$$

as a function of the control parameter $\eta = \kappa(N - 1)/\epsilon$ with $0 \leq \eta < \infty$. The corresponding energy surface is given by

$$\mathcal{E}(\beta, \gamma) = \frac{V_1(\beta) + V_3(\beta, \gamma)}{N\epsilon} = \frac{\beta^2}{1 + \beta^2} - \frac{\eta}{(1 + \beta^2)^2} \left[4\beta^2 \pm 2\sqrt{2}\beta^3 \cos 3\gamma + \frac{1}{2}\beta^4 \right], \quad (25)$$

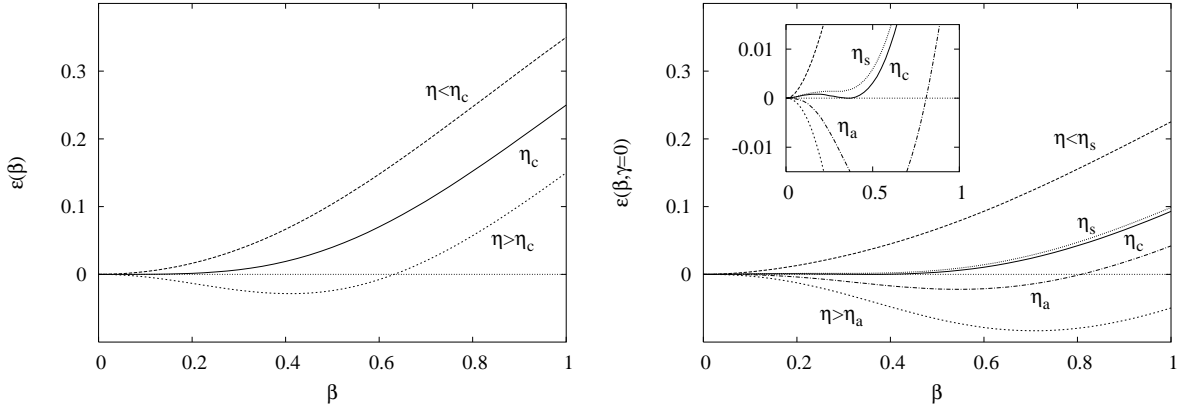


Figure 1: Potential-energy surfaces. (left) The second-order $U(5) - SO(6)$ phase transition: $\eta < \eta_c$ (dashed), $\eta = \eta_c$ (solid) and $\eta > \eta_c$ (short-dashed). (right) The first-order $U(5) - SU(3)$ phase transition: $\eta < \eta_s$ (dashed), $\eta = \eta_s$ (dotted), $\eta = \eta_c$ (solid), $\eta = \eta_a$ (dotted-dashed) and $\eta > \eta_a$ (short-dashed).

where the energy functionals of Eqs. (10) and (14) are scaled by ϵ and the number of bosons N . The analysis of the ground state energy as a function of η is more complicated than in the previous case due to the presence of the $\beta^3 \cos 3\gamma$ term. It was found that H_{13} exhibits a first-order phase transition at the critical point $\eta_c = 2/9$ [4].

An analysis with catastrophe shows that the values of the coefficients r_1 and r_2 for H_{13} are given by

$$r_1 = \frac{1 - 4\eta}{1 + 3\eta}, \quad r_2 = \frac{\pm 4\sqrt{2}\eta}{1 + 3\eta}, \quad (26)$$

from which it is easy to see that the transitional region between the $U(5)$ and $SU(3)$ limits is characterized by a straight line

$$r_1 = 1 \mp \frac{7}{4\sqrt{2}}r_2, \quad -\frac{4}{3} \leq r_1 \leq 1. \quad (27)$$

The critical, antispinodal and spinodal points are obtained by taking the intersection of the straight line of Eq. (27) with the curves corresponding to Eqs. (16) and (17). The critical point is characterized by

$$\eta_c = \frac{2}{9}, \quad r_{1c} = \frac{1}{15}, \quad r_{2c} = \pm \frac{8\sqrt{2}}{15}. \quad (28)$$

The equilibrium value of the deformation parameter at the critical point is given by [8]

$$\beta_c = \frac{r_{2,c}}{1 + \sqrt{1 + r_{2,c}^2/2}} = \frac{1}{2\sqrt{2}}, \quad (29)$$

in agreement with [4]. For the antispinodal point one finds

$$\eta_a = \frac{1}{4}, \quad r_{1a} = 0, \quad r_{2a} = \pm \frac{4\sqrt{2}}{7}. \quad (30)$$

The expressions for the spinodal point are rather complicated, which is the reason why only numerical values are given

$$\eta_s = 0.219 , \quad r_{1s} = 0.075 , \quad r_{2s} = \pm 0.748 . \quad (31)$$

In the right panel of Fig. 1 the potential-energy surface is given for five different values of the control parameter η . For $0 \leq \eta < \eta_s$ the system only has a spherical minimum. At $\eta = \eta_s$, it develops a second deformed minimum which becomes degenerate with the spherical minimum at $\eta = \eta_c$. The spherical minimum disappears at $\eta = \eta_a$, and for $\eta > \eta_a$ the system is deformed. For $\eta_s < \eta < \eta_a$, there is a coexistence of a spherical and a deformed minimum (see inset), the former is the lowest for $\eta_s < \eta < \eta_c$, and the latter for $\eta_c < \eta < \eta_a$. These features are characteristic of a first-order phase transition. Recent experiments have provided strong evidence for ^{152}Sm as a nucleus at the critical point of a phase transition between spherical and deformed shapes [14].

The $SO(6) - SU(3)$ transitional region

Finally, the transitional region between the $SO(6)$ and $SU(3)$ limits can be studied by

$$H_{23} = H_2 + H_3 = -\kappa' \hat{Q}(0) \cdot \hat{Q}(0) - \kappa \hat{Q}(\chi) \cdot \hat{Q}(\chi) , \quad \chi = \mp \frac{1}{2} \sqrt{7} . \quad (32)$$

as a function of the control parameter $\xi = \kappa/\kappa'$ with $0 \leq \xi < \infty$. The corresponding energy surface is given by

$$\begin{aligned} \mathcal{E}(\beta, \gamma) &= \frac{V_2(\beta) + V_3(\beta, \gamma)}{N(N-1)\kappa'} \\ &= -\frac{4\beta^2}{(1+\beta^2)^2} - \frac{\xi}{(1+\beta^2)^2} \left[4\beta^2 \pm 2\sqrt{2}\beta^3 \cos 3\gamma + \frac{1}{2}\beta^4 \right] , \end{aligned} \quad (33)$$

where the energy functionals of Eqs. (12) and (14) are scaled by $N(N-1)\kappa'$. In this case, there is no phase transition [4].

In terms of the coefficients r_1 and r_2 one finds

$$r_1 = -\frac{4+4\xi}{4+3\xi} , \quad r_2 = \pm \frac{4\xi\sqrt{2}}{4+3\xi} . \quad (34)$$

Also this transition corresponds to a straight line in the r_2 - r_1 plane

$$r_1 = -1 \mp \frac{r_2}{4\sqrt{2}} , \quad -\frac{4}{3} \leq r_1 \leq -1 . \quad (35)$$

Since the line defined in Eq. (35) does not intersect the curves for the critical, spinodal and antispinodal points, H_{23} does not exhibit a phase transition.

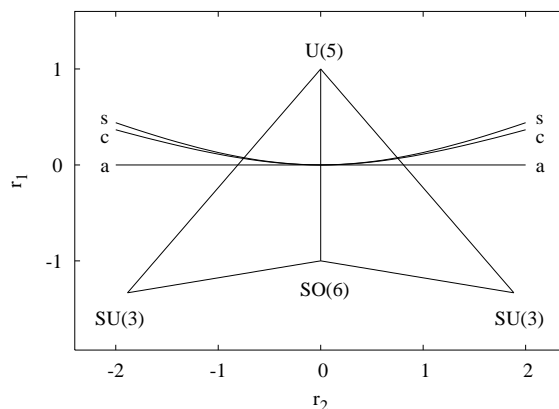


Figure 2: Shape-phase diagram for the IBM as a function of r_1 and r_2 . The curves marked by c , s and a correspond to the critical, spinodal and antispinodal points, respectively.

2.5 Shape-phase diagram

In Fig. 2, the results of the previous section are summarized in terms of a shape-phase diagram of the IBM plotted as a function of the coefficients r_1 and r_2 of Eq. (15). These coefficients are determined by the parameters of the Hamiltonian and completely classify the corresponding geometric shapes. A given Hamiltonian corresponds to a point in the r_2 - r_1 plane. However, note that the opposite is not true: a given point in the r_2 - r_1 plane corresponds not to a single Hamiltonian, but to a class of Hamiltonians which all share the same potential-energy surface, but differ in their kinetic energies.

The transitional regions between the dynamical symmetries form a kite (or a double triangle) spanned by the straight lines derived for each one of them, see Eqs. (22), (27) and (35). The dynamical symmetries occur at the end points of the kite, $U(5)$ (spherical), $SO(6)$ (γ -unstable deformed) and $SU(3)$ (prolate and oblate deformed). The critical points for the phase transition between spherical and deformed nuclei all lie on the curve defined by Eq. (16) which is labeled by “ c ” in Fig. 2. The spinodal and antispinodal points are labeled by “ s ” and “ a ”, respectively.

The region above the spinodal points ($r_1 > r_{1s}$) corresponds to spherical equilibrium shapes with only a spherical minimum. At the spinodal point ($r_1 = r_{1s}$), the system develops a second deformed minimum which becomes degenerate with the spherical minimum at the critical point ($r_1 = r_{1c}$). At the antispinodal point ($r_1 = r_{1a}$), the spherical minimum disappears and the region below the antispinodal points ($r_1 < r_{1a}$) corresponds to deformed equilibrium shapes with only a deformed minimum. For $r_{1s} < r_1 < r_{1a}$, there is a coexistence of a spherical and a deformed minimum, the former is the lowest for $r_{1s} < r_1 < r_{1c}$ and the latter for $r_{1c} < r_1 < r_{1a}$. These are the characteristic features of a first-order phase transition. On the line $r_2 = 0$, the spinodal, critical and antispinodal points coincide, corresponding to an isolated point with a second-order phase transition. The line $r_2 = 0$ and $r_1 < 0$ has been identified with a first-order quantum phase transition for γ -soft nuclei [8, 15].

An often-used representation of the phase space of the IBM is the so-called symmetry or Casten triangle which was introduced in [16] as a schematic way to represent the properties of the Hamiltonian: the dynamical symmetries at the corners, the transitions between two of them

along the sides, and arbitrary combinations of the three of them in the inside of the triangle [2]. In Section 2.4 it was shown that the catastrophe theory treatment of [8] provides a derivation of this triangle, not as a schematic representation, but as a function of two control parameters r_1 and r_2 which depend on the parameters of the Hamiltonian. This method is valid not only for the schematic Hamiltonian discussed in this contribution, but also for arbitrary IBM Hamiltonians.

2.6 Shape-phase coexistence

For first-order phase transitions between spherical and deformed shapes there is a very small region of coexistence. The right panel of Fig. 1 shows that the barrier that separates the spherical and deformed minima is very small, even in the inset it is hard to see. The height of the barrier is only a few percent of the excitation energy of the 2_1^+ state. In a recent study, evidence has been presented for the existence of such coexisting phases at low energy in the transitional nucleus ^{152}Sm [14].

However, it is important to distinguish between this type of shape coexistence which occurs for spherical-deformed transitional nuclei and the far more common phenomenon of coexisting shapes due to different configurations [3, 17]. The latter situations have been treated in an extension of the IBM in terms of a configuration mixing calculation, in which the normal and intruder configurations are described by IBM Hamiltonians and the configuration mixing by a coupling term [18]

$$\begin{pmatrix} H_{\text{normal}} & V_{\text{mix}} \\ V_{\text{mix}} & H_{\text{intruder}} \end{pmatrix}. \quad (36)$$

In this subsection, I briefly discuss some recent results obtained for the Ge isotopes [19, 20]. The even-even Ge isotopes show strong evidence for the coexistence of different geometric shapes. A sensitive probe for the configuration mixing is provided by two-neutron transfer reactions (p, t) and (t, p) , in particular the ratio of cross sections for the excitation of the 0_2^+ state and the ground state

$$R = \frac{\sigma(0_2^+ \rightarrow 0_1^+)}{\sigma(0_1^+ \rightarrow 0_1^+)}. \quad (37)$$

In the absence of mixing, this ratio is zero ($U(5)$ limit) or very small ($SU(3)$ and $SO(6)$ limits) [21]. However, if the two configurations are strongly mixed, R can be different from zero. In Fig. 3, I show the results for (p, t) and (t, p) reactions between the Ge isotopes [20]. The enhancement in the cross sections around $N = 40$ is an indication of the importance of configuration mixing.

2.7 Triaxial degrees of freedom

The one- and two-body IBM-1 Hamiltonian can give rise to spherical, axially deformed and γ -unstable deformed shapes. There is no stable triaxially deformed shape, unless one includes three-body interactions [22]. In the IBM-2 in which one distinguishes between protons and neutrons, there is in addition to the $U(5)$, $SU(3)$ and $SO(6)$ limits, another dynamical symmetry called the $SU^*(3)$ limit, which has been associated with triaxial shapes [23]. It is therefore

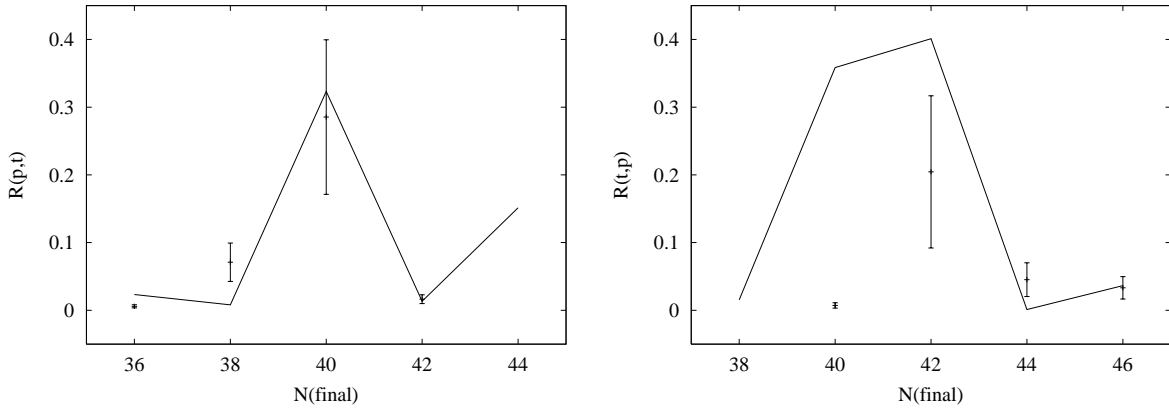


Figure 3: Comparison between experimental and theoretical cross sections for two-neutron transfer reactions (p,t) and (t,p) between Ge isotopes. N denotes the number of neutrons in the final Ge nucleus.

of great interest to extend the discussion of phase transitions to IBM-2, since there are new transitional regions which are not present in IBM-1, namely $U(5) - SU^*(3)$, $SU(3) - SU^*(3)$ and $SO(6) - SU^*(3)$. Let's consider a schematic IBM-2 Hamiltonian

$$H = \epsilon (n_{d_\pi} + n_{d_\nu}) - \kappa [Q_\pi(\chi_\pi) + Q_\nu(\chi_\nu)] \cdot [Q_\pi(\chi_\pi) + Q_\nu(\chi_\nu)] , \quad (38)$$

consisting of the d -boson energies and a quadrupole-quadrupole interaction. The $SU^*(3)$ limit arises for $\epsilon = 0$ and $\chi_\pi = -\chi_\nu = \pm\sqrt{7}/2$.

The analysis of the equilibrium shapes becomes a lot more complicated since in general one now has to study the properties of an energy surface that depends on 7 geometric variables: β_π , γ_π , (β_ν, γ_ν) for the geometry of the proton (neutron) distribution and three Euler angles $(\Theta) \equiv (\Theta_1, \Theta_2, \Theta_3)$ for the relative orientation of the proton and the neutron distributions. The general form of the potential-energy surface of IBM-2 can be found in [24]. In the same reference it was shown that only IBM-2 Hamiltonians with a repulsive hexadecupole-hexadecupole interaction can give rise to so-called oblique shapes, *i.e.* an equilibrium shape with $\Theta \neq 0$. Therefore, for the Hamiltonian of Eq. (38) one can take $\Theta = 0$ [25, 26]. The energy surface is then given by the simplified form

$$\begin{aligned} V(\beta_\pi, \gamma_\pi, \beta_\nu, \gamma_\nu) &= V(\beta_\pi, \gamma_\pi) + V(\beta_\nu, \gamma_\nu) \\ &\quad - \frac{2\kappa N_\pi N_\nu \beta_\pi \beta_\nu}{(1 + \beta_\pi^2)(1 + \beta_\nu^2)} \left[4 \cos(\gamma_\pi - \gamma_\nu) - 2\sqrt{\frac{2}{7}} \chi_\nu \beta_\nu \cos(\gamma_\pi + 2\gamma_\nu) \right. \\ &\quad \left. - 2\sqrt{\frac{2}{7}} \chi_\pi \beta_\pi \cos(\gamma_\nu + 2\gamma_\pi) + \frac{2}{7} \chi_\pi \chi_\nu \beta_\pi \beta_\nu \cos(2\gamma_\pi - 2\gamma_\nu) \right] , \quad (39) \end{aligned}$$

where $V(\beta_\rho, \gamma_\rho)$ is the energy surface for the proton ($\rho = \pi$) and the neutron ($\rho = \nu$) part of the Hamiltonian, see Eq. (6).

The results that have been obtained so far for IBM-2 are mostly numerical [25, 26]: there is a second-order phase transition for $U(5) - SU^*(3)$ and $SU(3) - SU^*(3)$, whereas for $SO(6) - SU^*(3)$ there is no phase transition. It would be very interesting to have analytic results for the phase

transitions between the four dynamical symmetries of the IBM-2. In this respect, the methods of catastrophe theory could be of help to obtain closed expressions for the critical and (anti)spinodal points, to provide insight into the order of the new phase transitions, and perhaps even to derive a shape-phase diagram for IBM-2, much in the same way as was done for the IBM-1 [8].

3 Random interactions

A different method to study the geometric shapes of the IBM, and especially their robustness, is that of Hamiltonians with random interactions.

Random matrix theory was developed to describe statistical properties of nuclear spectra, such as average distributions and fluctuations of peaks in neutron-capture experiments [27, 28]. In this approach, the Hamiltonian matrix elements are chosen at random, while keeping some global symmetries, *i.e.* the matrix should be hermitean, and be invariant under time-reversal, rotations and reflections. Specific examples include the Gaussian Orthogonal Ensemble (GOE) of real-symmetric random Hamiltonian matrices in which the many-body interactions are uncorrelated, and the Two-Body Random Ensemble (TBRE) in which the two-body interactions are taken from a distribution of random numbers [29]. For two-particle systems the two ensembles are identical but for more than two particles, unlike in the case of GOE, in TBRE the many-body matrix elements are correlated. As a consequence, also the energy eigenvalues of states with different quantum numbers are strongly correlated, since they arise from the same Hamiltonian.

The latter aspect was investigated in shell model calculations for even-even nuclei in the *sd* shell and the *pf* shell [30]. An analysis of the energy spectra of an ensemble of random two-body Hamiltonians showed a remarkable statistical preference for ground states with angular momentum and parity $L^P = 0^+$, despite the random nature of the two-body matrix elements both in sign and relative magnitude. A similar preponderance of 0^+ ground states was found in an analysis of the IBM with random interactions [31]. In addition, in the IBM evidence was found for both vibrational and rotational band structures. According to the conventional ideas in the field, the occurrence of $L = 0$ ground states and the existence of vibrational and rotational bands are due to very specific forms of the interactions. Therefore, these unexpected and surprising results with random interactions have sparked a large number of investigations to explain and further explore the properties of random nuclei (see *e.g.* the reviews by Bijker and Frank [32], Zelevinsky and Volya [33] and Zhao, Arima and Yoshinaga [34]).

In this section, I discuss the phenomenon of emerging regular spectral features from the IBM with random interactions and its relation with the underlying geometric shapes and critical points.

3.1 Regular features and robust results

In order to study the geometric shapes associated with the IBM, let's consider the most general one- and two-body IBM Hamiltonian

$$H = \frac{1}{N} \left[H_{1,b} + \frac{1}{N-1} H_{2,b} \right], \quad (40)$$

where $H_{1,b}$ contains the boson energies

$$H_{1,b} = \epsilon_s s^\dagger \cdot \tilde{s} + \epsilon_d d^\dagger \cdot \tilde{d}, \quad (41)$$

and $H_{2,b}$ the two-body interactions

$$\begin{aligned} H_{2,b} = & u_0 \frac{1}{2} (s^\dagger \times s^\dagger)^{(0)} \cdot (\tilde{s} \times \tilde{s})^{(0)} + u_2 (s^\dagger \times d^\dagger)^{(2)} \cdot (\tilde{d} \times \tilde{s})^{(2)} \\ & + \sum_{\lambda=0,2,4} c_\lambda \frac{1}{2} (d^\dagger \times d^\dagger)^{(\lambda)} \cdot (\tilde{d} \times \tilde{d})^{(\lambda)} \\ & + v_0 \frac{1}{2\sqrt{2}} \left[(d^\dagger \times d^\dagger)^{(0)} \cdot (\tilde{s} \times \tilde{s})^{(0)} + (s^\dagger \times s^\dagger)^{(0)} \cdot (\tilde{d} \times \tilde{d})^{(0)} \right] \\ & + v_2 \frac{1}{2} \left[(d^\dagger \times d^\dagger)^{(2)} \cdot (\tilde{d} \times \tilde{s})^{(2)} + (s^\dagger \times d^\dagger)^{(2)} \cdot (\tilde{d} \times \tilde{d})^{(2)} \right]. \end{aligned} \quad (42)$$

The nine parameters of the IBM Hamiltonian of Eqs. (40)-(42), altogether denoted by

$$(\vec{x}) \equiv (\epsilon_s, \epsilon_d, u_0, u_2, c_0, c_2, c_4, v_0, v_2), \quad (43)$$

are taken as independent random numbers x_i ($i = 1, \dots, 9$) on a Gaussian distribution

$$P(x_i) = e^{-x_i^2/2\sigma^2} / \sigma\sqrt{2\pi}, \quad (44)$$

with zero mean and width σ . In this way, the interaction terms are arbitrary and equally likely to be attractive or repulsive. The spectral properties of each Hamiltonian are then analyzed by exact numerical diagonalization [31].

The properties of the energy spectra can be studied by the energy ratio

$$R_{4/2} = \frac{E(4_1^+) - E(0_1^+)}{E(2_1^+) - E(0_1^+)}. \quad (45)$$

In Table 2, the values of $R_{4/2}$ are presented for each of the dynamical symmetries: $R_{4/2} = 2.0$, 2.5 and 3.3 for the $U(5)$, $SO(6)$ and $SU(3)$ limits, respectively. Fig. 4 shows a remarkable result: the probability distribution $P(R_{4/2})$ has two very pronounced peaks, one at ~ 1.95 and a narrower one at ~ 3.35 . These values correspond almost exactly to the harmonic vibrator and rotor values (see the results for the $U(5)$ and $SU(3)$ limits in Table 2). No such peak is observed for the γ -unstable or deformed oscillator case ($SO(6)$ limit). This can be understood from the fact that γ dependence of the potential-energy surface arises from a single parameter, v_2 . For a γ -unstable solution to occur, v_2 has to be zero. For $v_2 \neq 0$ the energy surface has a prolate or an oblate minimum (whether the global minimum is spherical or deformed depends on the other terms in the Hamiltonian as well).

Energies by themselves are not sufficient to decide whether or not there exists band structure. Levels belonging to a collective band are connected by strong electromagnetic transitions. In Fig. 4 a correlation plot is shown between the ratio of $B(E2)$ values for the $4_1^+ \rightarrow 2_1^+$ and $2_1^+ \rightarrow 0_1^+$ transitions and the energy ratio $R_{4/2}$. Table 2 shows that in the large N limit this ratio of $B(E2)$ values is 2 for the harmonic oscillator ($U(5)$ limit) and 10/7 for the deformed

Table 2: Energies of $B(E2)$ values in the dynamical symmetry limits of the IBM for the Hamiltonians of Eqs. (9), (11) and (13).

| | $\frac{E(4_1^+) - E(0_1^+)}{E(2_1^+) - E(0_1^+)}$ | $\frac{E(0_2^+) - E(0_1^+)}{E(2_1^+) - E(0_1^+)}$ | $\frac{B(E2;4_1^+ \rightarrow 2_1^+)}{B(E2;2_1^+ \rightarrow 0_1^+)}$ |
|---------|---|---|---|
| $U(5)$ | 2 | 2 | $\frac{2(N-1)}{N} \rightarrow 2$ |
| $SO(6)$ | $\frac{5}{2}$ | $N + 1$ | $\frac{10(N-1)(N+5)}{7N(N+4)} \rightarrow \frac{10}{7}$ |
| $SU(3)$ | $\frac{10}{3}$ | $\frac{4(2N-1)}{3}$ | $\frac{10(N-1)(2N+5)}{7N(2N+3)} \rightarrow \frac{10}{7}$ |

oscillator and the rotor ($SO(6)$ and $SU(3)$ limit, respectively). The right panel of Fig. 4 shows a strong correlation between the first peak in the energy ratio and the vibrator value for the ratio of $B(E2)$ values (the concentration of points in this region corresponds to about 50 % of all cases), as well as for the second peak and the rotor value (about 25 % of all cases).

Despite the random nature of the interaction strengths both in relative size and sign, the ground state still has $L = 0$ in the majority of the cases. Fig. 5 shows the percentages of ground states with $L = 0$ and $L = 2$ as a function of the boson number N (solid line). One sees a clear dominance of ground states with $L = 0$ with ~ 60 -75%. For $N = 3k$ (a multiple of 3) one sees an enhancement for $L = 0$ and a decrease for $L = 2$. The sum of the two hardly depends on the number of bosons.

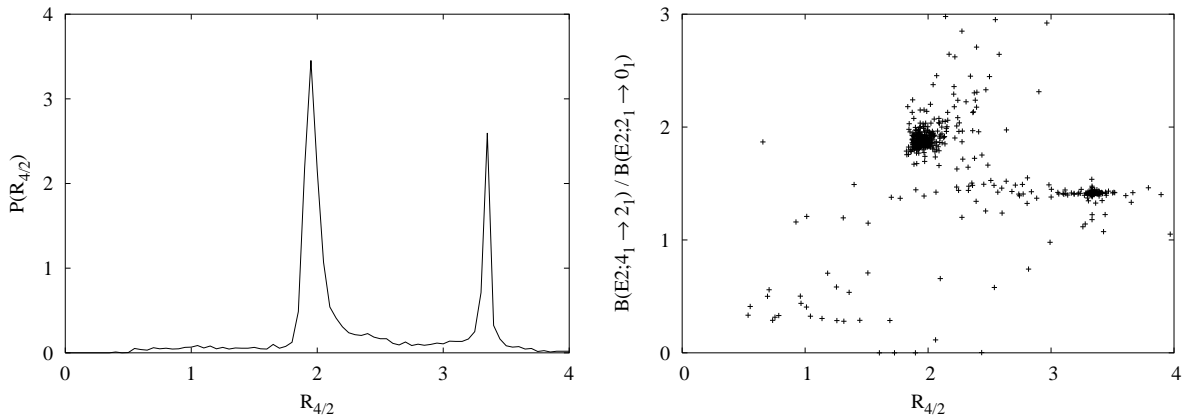


Figure 4: Probability distribution $P(R_{4/2})$ of the energy ratio $R_{4/2}$ (left) and correlation between ratios of $B(E2)$ values and energies (right) for the IBM with random one- and two-body interactions. The number of bosons is $N = 16$.

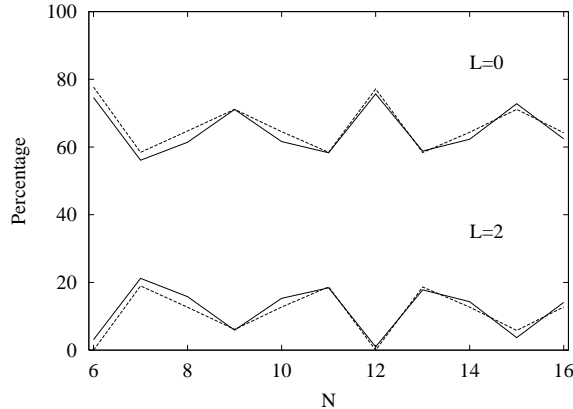


Figure 5: Percentages of ground states with $L = 0$ (top) and $L = 2$ (bottom) in the IBM with random one- and two-body interactions as a function of the number of bosons N : calculated exactly for 10,000 runs (solid line) and in mean-field approximation (dashed line).

3.2 Mean-field analysis

The results obtained in studies of the nuclear shell model and the IBM with random interactions are very surprising and unexpected in the sense that, according to the conventional ideas in the field, the occurrence of $L = 0$ ground states and the existence of vibrational and rotational bands are due to very specific forms of the interactions.

The basic ingredients of the numerical simulations are the structure of the model space, the ensemble of random Hamiltonians, the order of the interactions (one- and two-body), and the global symmetries, *i.e.* time-reversal, hermiticity and rotation and reflection symmetry. The latter three symmetries cannot be modified, since nuclear levels have real energies and good angular momentum and parity. It has been shown that the observed spectral order is a robust property that does not depend on the specific choice of the ensemble of random interactions [30, 35, 36], the time-reversal symmetry [35], or the restriction of the Hamiltonian to one- and two-body interactions [37]. These results suggest that that an explanation of the origin of the observed regular features has to be sought in the many-body dynamics of the model space and/or the general statistical properties of random interactions.

In this section, the origin of the regular features that emerge from random interactions in the IBM [38] are studied using standard Hartree-Bose mean-field methods [39] in which the trial wave function is the boson condensate of Eqs. (4) and (5) (see Section 2.2).

Vibrations

The potential-energy surface associated with the IBM Hamiltonian of Eqs. (40)-(42) is given by its expectation value in the coherent state

$$V(\beta, \gamma) = a_0 + a_2 \frac{\beta^2}{1 + \beta^2} \frac{1}{(1 + \beta^2)^2} \left[a_3 \beta^3 \cos 3\gamma + a_4 \beta^4 \right], \quad (46)$$

where the coefficients a_i are linear combinations of the parameters of the Hamiltonian

$$\begin{aligned}
a_4 &= \frac{1}{2}u_0 - u_2 + \frac{1}{10}c_0 + \frac{1}{7}c_2 + \frac{9}{35}c_4 - \frac{1}{\sqrt{10}}v_0, \\
a_3 &= -\sqrt{\frac{2}{7}}v_2, \\
a_2 &= \epsilon_d - \epsilon_s - u_0 + u_2 + \frac{1}{\sqrt{10}}v_0, \\
a_0 &= \epsilon_s + \frac{1}{2}u_0.
\end{aligned} \tag{47}$$

The energy surface of Eq. (46) provides information on the distribution of shapes that the model can acquire. The values of β_e and γ_e that characterize the equilibrium configuration of the potential-energy surface depend on the coefficients a_4 , a_3 and a_2 . The equilibrium shapes can be divided into three different classes:

- $\beta_e = 0$: an s -boson or spherical condensate
- $0 < \beta_e < \infty$ with $\gamma = 0^\circ$ or $\gamma = 60^\circ$: a deformed condensate with prolate or oblate symmetry, respectively, and
- $\beta_e = \infty$: a d -boson condensate.

Rotations

Each equilibrium configuration has its own characteristic angular momentum content. Even though the angular momentum states are not projected from the coherent state, the ground state angular momentum can be obtained from the rotational structure of the condensate in combination with the Thouless-Valatin formula for the corresponding moments of inertia. This procedure is described in detail in [39]. The application to the IBM with random interactions leads to the following results.

- The s -boson condensate corresponds to a spherical shape. Whenever such a condensate occurs (in 39.4 % of the cases), the ground state has $L = 0$.
- The deformed condensate corresponds to an axially symmetric deformed rotor. The ordering of the rotational energy levels $L = 0, 2, \dots, 2N$ is determined by the sign of the moment of inertia

$$E_{\text{rot}} = \frac{1}{2\mathcal{I}_3}L(L+1). \tag{48}$$

The moment of inertia \mathcal{I}_3 depends in a complicated way on the parameters in the Hamiltonian. The deformed condensate occurs in 36.8 % of the cases. For $\mathcal{I}_3 > 0$ the ground state has $L = 0$ (23.7 %), while for $\mathcal{I}_3 < 0$ the ground state has the maximum value of the angular momentum $L = 2N$ (13.1 %).

- The d -boson condensate corresponds to a quadrupole oscillator with N quanta. Its rotational structure has a more complicated structure, since the rotational excitation energies depend on two moments of inertia

$$E_{\text{rot}} = \frac{1}{2\mathcal{I}_5}\tau(\tau + 3) + \left(\frac{1}{2\mathcal{I}_3} - \frac{1}{6\mathcal{I}_5} \right) L(L + 1), \quad (49)$$

which are associated with the spontaneously broken three- and five-dimensional rotational symmetries of the d -boson condensate. The d -boson condensate occurs in the remaining 23.8 % of the cases. The results in Table 3 can be understood qualitatively as follows. For $\mathcal{I}_5 > 0$ the ground state has $\tau = 0$ for N even or $\tau = 1$ for N odd (~ 4 %), while for $\mathcal{I}_5 < 0$ the ground state has the maximum value of the boson seniority $\tau = N$ (~ 19 %). For $\tau = 0$ and $\tau = 1$ there is a single angular momentum state with $L = 0$ and $L = 2$, respectively. For the $\tau = N$ multiplet, the angular momentum of the ground state depends on the sign of the moment of inertia \mathcal{I}_3 . For $\mathcal{I}_3 > 0$ the ground state has $L = 0$ for $N = 3k$ or $L = 2$ for $N \neq 3k$ (9 %), while for $\mathcal{I}_3 < 0$ the ground state has the maximum value of the angular momentum $L = 2N$ (10 %).

Table 3 shows that the spherical and deformed condensates contribute constant amounts of 39.4 % and 23.7 %, respectively, to the $L = 0$ ground state percentage, whereas the contribution from the d -boson condensate depends on the number of bosons N . The $L = 2$ ground states arise completely from the d -boson condensate solution. Fig. 5 shows the percentages of ground states with $L = 0$ and $L = 2$ as a function of the total number of bosons N . A comparison of the results of the mean-field analysis (dashed lines) and the exact ones (solid lines) shows an excellent agreement. There is a dominance of ground states with $L = 0$ for ~ 63 -77 % of the cases. Both for $L = 0$ and $L = 2$ there are large oscillations with N which are entirely due to the contribution of the d -boson condensate. For $N = 3k$ one sees an enhancement for $L = 0$

Table 3: Percentages of ground states with $L = 0, 2$ and $2N$, obtained in a mean-field analysis of the IBM.

| Shape | $L = 0$ | $L = 2$ | $L = 2N$ | |
|------------------------|---------|---------|----------|----------------------|
| $\beta_e = 0$ | 39.4 % | 0.0 % | 0.0 % | |
| $0 < \beta_e < \infty$ | 23.7 % | 0.0 % | 13.1 % | |
| $\beta_e = \infty$ | 13.5 % | 0.0 % | 10.3 % | $N = 6k$ |
| | 0.2 % | 13.2 % | 10.4 % | $N = 6k + 1, 6k + 5$ |
| | 4.4 % | 9.0 % | 10.4 % | $N = 6k + 2, 6k + 4$ |
| | 9.3 % | 4.0 % | 10.5 % | $N = 6k + 3$ |

and a corresponding decrease for $L = 2$. In the mean-field analysis, the sum of the two which accounts for $\sim 77\%$ of the cases, hardly depends on the number of bosons, in agreement with the exact results. For the remaining $\sim 23\%$ of the cases, the ground state has the maximum value of the angular momentum $L = 2N$.

In conclusion, the emergence of regular features from the IBM with random interactions can be explained in a Hartree-Bose mean-field analysis of the random ensemble of Hamiltonians, in which different regions of the parameter space are associated with particular intrinsic states, which in turn correspond to definite geometric shapes [38]. There are three solutions: a spherical shape carried by a single state with $L = 0$, a deformed shape which corresponds to a rotational band with $L = 0, 2, \dots, 2N$, and a condensate of quadrupole bosons which has a more complicated angular momentum content. The ordering of rotational energy levels depends on the sign of the corresponding moments of inertia. The mean-field analysis explains both the distribution of ground state angular momenta and the occurrence of vibrational and rotational bands. The same conclusions hold for the vibron model for which a large part of the results has been obtained analytically [40].

3.3 Evolution of quasi-beta energies

Recently, an interesting empirical correlation was pointed out [41] between $R_{4/2}$ of Eq. (45) and

$$R_{0/2} = \frac{E(0_2^+) - E(0_1^+)}{E(2_1^+) - E(0_1^+)}. \quad (50)$$

The left panel of Fig. 6 shows the experimental values for the nuclei with neutron number $84 \leq N \leq 96$ and the right panel the results of a IBM calculation in which the parameters of the CQF Hamiltonian of Eq. (1) are taken randomly, but are restricted to the physically allowed region, *i.e.* $\epsilon > 0$, $\kappa > 0$ and $-\sqrt{7}/2 \leq \chi \leq \sqrt{7}/2$. For vibrational nuclei both energy ratios are equal to 2, since the 0_2^+ and 4_1^+ states belong to the two-phonon multiplet, whereas for rotational nuclei the 4_1^+ state is a rotational excitation and the 0_2^+ state a vibrational excitation

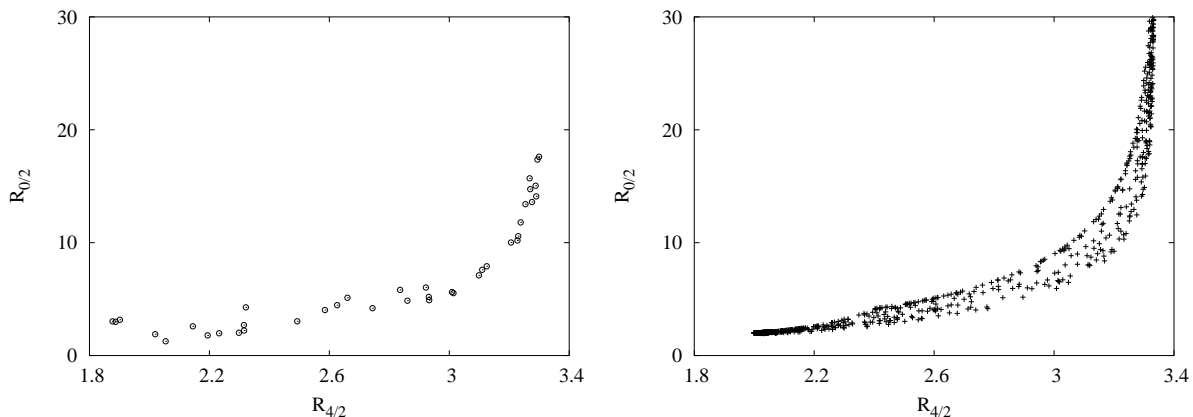


Figure 6: Correlation plot between the energy ratios $R_{0/2}$ and $R_{4/2}$: (left) experimental values [41] and (right) theoretical values calculated in the consistent Q-formulation of the IBM.

Table 4: Comparison of energy ratios for the critical points of the IBM Hamiltonians H_{12} and H_{13} with $N = 11$ and the critical point symmetries [2].

| | $U(5) - SO(6)$ $\eta_c = 1/4$ | $E(5)$ | $U(5) - SU(3)$ $\eta_c = 2/9$ | $X(5)$ |
|-----------|----------------------------------|--------|----------------------------------|--------|
| $R_{4/2}$ | 2.22 | 2.20 | 2.33 | 2.91 |
| $R_{0/2}$ | 2.61 | 3.03 | 2.41 | 5.67 |

(see Table 2). Fig. 6 shows that this trend is satisfied both by the data and by schematic IBM calculations in which only some minimal restrictions are imposed upon the Hamiltonian.

3.4 Signatures of critical point nuclei

Finally, I briefly address the question of experimental signatures of critical point nuclei [10]. Phase transitions in nuclei can be tested experimentally by measuring observables that are particularly sensitive to them, such as separation energies S_{2n} , isomer shifts $\delta\langle r^2 \rangle$ and the transition rates $B(E2; 2_3^+ \rightarrow 0_2^+)$ [14]. Other observables that have been suggested as measures of critical point nuclei are the energy ratios $R_{4/2}$ and $R_{0/2}$. Table 4 shows the values of these ratios for the IBM Hamiltonians H_{12} and H_{13} at the critical points $\eta_c = 1/4$ and $\eta_c = 2/9$, respectively. A comparison with the values for the critical point symmetries, $E(5)$ and $X(5)$ [2], shows that the energy ratios for the critical points in the IBM are rather different from the those for the critical point symmetries. This is not so surprising, since the potential-energy surfaces for IBM Hamiltonians at the critical points are not square-well potentials (see Fig. 1) as in the critical point symmetries [2]. Moreover, one has to take into account that there is an entire class of IBM Hamiltonians which all share the same potential-energy surface and hence have the same critical points, but differ in their kinetic energies. Therefore, there is not a single value of the energy ratios $R_{4/2}$ and $R_{0/2}$ that can be used to identify a nucleus as a "critical point" nucleus. Instead one should rather study the change in energy ratios, $B(E2)$ values and/or quadrupole moments in a chain of nuclei to determine whether these nuclei exhibit a shape-phase transition.

4 Summary, conclusions and outlook

In these lecture notes I have presented a review of shape-phase transitions in nuclei and random interactions. Maybe at first sight, these two topics have little to do with one another, but both were shown to provide evidence for the existence of robust shapes in collective nuclei. The transitions between different shapes occur very rapidly, typically with the addition or removal of one or two pairs of nucleons.

An analysis in IBM-1 and IBM-2 showed that the phase transitions between spherical and axially deformed nuclei are of first order, whereas those between spherical and triaxially deformed

and between axially deformed and triaxially deformed are of second order.

Two-neutron transfer reactions (p, t) and (t, p) for the Ge isotopes were shown to provide a sensitive probe of shape-phase coexistence of a normal and an intruder configuration. In particular, the ratio of cross sections for the excitation of the first excited 0^+ state and the ground state is either very small or zero in the absence of configuration mixing, but may be enhanced for strongly mixed configurations.

The importance of the concept of geometric shapes in nuclei was confirmed by a study of the IBM with random interactions. Despite the random nature of the interactions a highly surprising degree of regularity was observed, in particular the dominance of ground states with $L = 0$ and the occurrence of vibrational and rotational band structures. It was shown that the geometric shapes associated with IBM Hamiltonians play a crucial role in understanding the origin of these regular properties. These shapes are a reflection of an intrinsic geometry associated to the many-body dynamics of the model space which is sampled by the statistical nature of the random interactions, but which is quite independent of them. The observed spectral order is a robust property that arises from a much larger class of Hamiltonians than is usually thought.

Acknowledgments

It is a pleasure to thank Pepe Arias, José Barea, Mark Caprio, Octavio Castaños, Rick Casten, Alejandro Frank, Franco Iachello, Elizabeth Padilla and Norbert Pietralla for interesting discussions. This work was supported in part by CONACyT.

References

- [1] See *e.g.* A.N. Andreyev *et al.*, Nature **405**, 430 (2000); D. Warner, Nature **420**, 614 (2002).
- [2] F. Iachello, Proceedings of the International School of Physics “Enrico Fermi”, Course CLIII, Eds. A. Molinari, L. Riccati, W.M. Alberico and M. Morando, (IOS Press, Amsterdam, 2003), 1-37.
- [3] See *e.g.* the reviews: K. Heyde, P. Van Isacker, M. Waroquier, J.L. Wood and R.A. Meyer, Phys. Rep. **102**, 291 (1983); J.L. Wood, K. Heyde, W. Nazarewicz, M. Huyse and P. van Duppen, Phys. Rep. **215**, 101 (1992).
- [4] A.E.L. Dieperink, O. Scholten and F. Iachello, Phys. Rev. Lett. **44**, 1747 (1980); A.E.L. Dieperink and O. Scholten, Nucl. Phys. A **346**, 125 (1980).
- [5] W.-M. Zhang, D.H. Feng and R. Gilmore, Rev. Mod. Phys. **62**, 867 (1990).
- [6] R. Gilmore, J. Math. Phys. **20**, 891 (1979).
- [7] D.H. Feng, R. Gilmore and S.R. Deans, Phys. Rev. C **23**, 1254 (1981).
- [8] E. López-Moreno and O. Castaños, Phys. Rev. C **54**, 2374 (1996); Rev. Mex. Fís. **49**, Suplemento 4, 15 (2003).

- [9] F. Iachello, Phys. Rev. Lett. **85**, 3580 (2000); *ibid.* **87**, 052502 (2001); *ibid.* **91**, 132502 (2003).
- [10] R.F. Casten, these proceedings.
- [11] F. Iachello and A. Arima, *The interacting boson model* (Cambridge University Press, 1987).
- [12] D.D. Warner and R.F. Casten, Phys. Rev. Lett. **48**, 1385 (1982).
- [13] R. Gilmore, *Catastrophe Theory for Scientists and Engineers* (Wiley, New York, 1981).
- [14] F. Iachello, N.V. Zamfir and R.F. Casten, Phys. Rev. Lett. **81**, 1191 (1998).
- [15] J. Jolie, R.F. Casten, P. von Brentano and V. Werner, Phys. Rev. Lett. **87**, 162501 (2001).
- [16] R.F. Casten, in *Interacting Bose-Fermi Systems in Nuclei*, Ed. F. Iachello, (Plenum Press, New York, 1981), p1.
- [17] K. Heyde, J. Jolie, R. Fossion, S. De Baerdemacker and V. Hellemans, Phys. Rev. C **69**, 054304 (2004).
- [18] P.D. Duval and B.R. Barrett, Nucl. Phys. A **376**, 213 (1982).
- [19] P.D. Duval, D. Goutte and M. Vergnes, Phys. Lett. B **124**, 297 (1983).
- [20] E. Padilla-Rodal, Ph.D. thesis, U.N.A.M., Mexico (2004).
- [21] A. Arima and F. Iachello, Phys. Rev. C **16**, 2085 (1977).
- [22] P. Van Isacker and J.-Q. Chen, Phys. Rev. C **24**, 684 (1981).
- [23] A.E.L. Dieperink and R. Bijker, Phys. Lett. B **116**, 77 (1982).
- [24] J.N. Ginocchio and A. Leviatan, Ann. Phys. (N.Y.) **216**, 152 (1992).
- [25] J.M. Arias, J.E. García-Ramos and J. Dukelsky, Phys. Rev. Lett. (2004), **93**, 212501 (2004).
- [26] M.A. Caprio and F. Iachello, Phys. Rev. Lett. **93**, 242502 (2004).
- [27] E.P. Wigner, Ann. of Math. **62**, 548 (1955); Ann. of Math. **67**, 325 (1958).
- [28] C.E. Porter, *Statistical Theories of Spectra: Fluctuations*, (Academic Press, New York, 1965).
- [29] T.A. Brody, J. Flores, J.B. French, P.A. Mello, A. Pandey and S.S.M. Wong, Rev. Mod. Phys. **53**, 385 (1981).
- [30] C.W. Johnson, G.F. Bertsch and D.J. Dean, Phys. Rev. Lett. **80**, 2749 (1998).
- [31] R. Bijker and A. Frank, Phys. Rev. Lett. **84**, 420 (2000).
- [32] R. Bijker and A. Frank, Nuclear Physics News, Vol. **11**, No. 4, 15 (2001).

- [33] V. Zelevinsky and A. Volya, Phys. Rep. **391**, 311 (2004).
- [34] Y.M. Zhao, A. Arima and N. Yoshinaga, Phys. Rep. **400**, 1 (2004).
- [35] R. Bijker, A. Frank and S. Pittel, Phys. Rev. C **60**, 021302 (1999).
- [36] C.W. Johnson, G.F. Bertsch, D.J. Dean and I. Talmi, Phys. Rev. C **61**, 014311 (2000).
- [37] R. Bijker and A. Frank, Phys. Rev. C **62**, 014303 (2000).
- [38] R. Bijker and A. Frank, Phys. Rev. C **64**, 061303 (2001).
- [39] J. Dukelsky, G.G. Dussel, R.P.J. Perazzo, S.L. Reich and H.M. Sofia, Nucl. Phys. A **425**, 93 (1984).
- [40] R. Bijker and A. Frank, Phys. Rev. C **65**, 044316 (2002).
- [41] N. Pietralla and O.M. Gorbachenko, Phys. Rev. C **70**, 011304 (2004); N. Pietralla, these proceedings.